Original Research Article

JOURNAL OF SANDWICH STRUCTURES & MATERIALS

Journal of Sandwich Structures & Materials
2026, Vol. 0(0) 1–26

DOI: 10.1177/10996362261489128
journals.sagepub.com/home/jsm
Sage

Investigation of a recyclable flax–acrylic composite structure (FLACS) for construction applications

Rui Pereira[1], Paulo Antunes[2] and Braian Uribe[1]

Abstract

Sandwich composite structures combine high stiffness, mechanical strength and low weight, making them attractive for panel applications in construction. However, their limited reprocessability, arising from the use of thermoset matrices that cannot be remelted after crosslinking, restricts their recyclability and sustainable use. This study reports the development of a recyclable sandwich composite structure based on flax fibers and a liquid polymethyl methacrylate (PMMA) thermoplastic matrix (FLACS). The work includes the fabrication of the core and face sheets, as well as the complete sandwich structure, using a combination of resin infusion and compression molding techniques. Mechanical testing revealed a bending strength of 41 MPa, a compressive load capacity of 19.6 kN and an energy absorption of 14.1 J under low-velocity impact. With a density of 234 kg/m^3, the material demonstrates high specific mechanical performance. FLACS was subsequently subjected to a single mechanical recycling cycle followed by thermo-mechanical processing, without the addition of virgin polymer. The results demonstrate the feasibility of recovering the material as feedstock for manufacturing new composite panels suitable for scalable construction applications.

Keywords

thermoplastic composites, natural fiber, honeycomb, circularity, lightweight construction, sandwich structure, mechanical behavior

[1]Institute for Polymers and Composites (IPC), University of Minho, Guimarães, Portugal
[2]Centre for Innovation in Polymer Engineering (PIEP), University of Minho, Guimarães, Portugal

Corresponding author:
Braian Uribe, Institute for Polymers and Composites (IPC), University of Minho, Campus Azurém, Guimarães 4800-058, Portugal.
Email: brianes@dep.uminho.pt

Introduction

Sandwich composite structures (SCSs)[1] have emerged as a critical class of engineered materials, offering exceptional stiffness-to-weight and strength-to-weight ratios that are difficult to achieve with conventional monolithic materials. Structurally, these composites consist of two thin, high-strength face sheets bonded to a lightweight, low-density core.[2,3] The primary advantage of sandwich structures lies in their ability to decouple bending and shear functions within a structure. The stiff outer face sheets resist in-plane tensile and compressive stresses, while the core primarily resists transverse shear and provides support to prevent local buckling of the face sheets.[3,4] This functional partitioning enables significant material savings and enhances structural efficiency.

Face sheets serve as the primary functions of supporting in-plane loads, protecting the core, and increasing the structural stiffness of the SCS by increasing the inertia moment of the section.[5,6] Face sheets are often fabricated from fiber-reinforced polymer composites (PMCs),[7–10] metals,[11] or ceramics,[12] depending on the performance requirements of the application.

From a design perspective, the selection of the core material is critical in defining the mechanical performance of sandwich composite structures. Polymeric foam cores provide advantages such as low cost, reduced weight and good energy absorption,[13] but they are often limited by lower mechanical strength.[14] In contrast, honeycomb cores—typically fabricated from aluminium or aramid paper—offer higher specific stiffness and strength, though their fabrication is more complex and costly.[10,15] Therefore, the choice of core material involves a trade-off between performance, weight, cost and fabrication complexity, depending on the specific requirements of the application. The main parts of a sandwich composite structures are presented in Figure 1.

In the construction sector, sandwich structures play a crucial role in improving the mechanical and thermal performance of buildings by being used in Structural Insulated Panels (SIPs)[16] and Prefabricated Modular Panels (PMPs).[17] These systems integrate lightweight cores—commonly polymer foams such as expanded or extruded polystyrene (EPS, XPS), polyurethane (PU), or polyisocyanurate (PIR)—with structural facings like oriented strand board (OSB), fiber-reinforced plastics, or metals.[18] Their combination results in panels that not only enhance thermal efficiency and mechanical stability but also enable rapid installation and reduced labor requirements, aligning with modern prefabrication trends. Despite their widespread adoption in walls, roofs, and facades, the heavy reliance on thermoset foams and non-recyclable facings poses significant challenges for sustainable end-of-life (EOL) management.

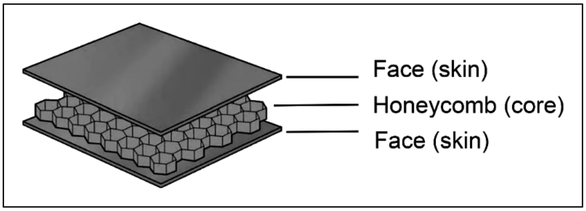

Figure 1. Main parts of a SCS.

The crosslinked architecture of thermosets hinders reprocessing,[19] while many thermoplastic foams present environmental risks to ecosystems and human health.[20,21] Moreover, the heterogeneous configuration of these composites, composed of dissimilar and tightly bonded layers, limits the feasibility of mechanical or chemical recycling. Consequently, end-of-life panels are often disposed of in landfills or incinerated, contributing to pollution and resource depletion.[19] Structural reuse is also constrained by damage at the core–interface level and the difficulty of non-destructive disassembly. These challenges have accelerated research toward recyclable, bio-based and modular sandwich systems designed to improve sustainability without compromising performance.[22–26]

To address the environmental limitations of traditional SCSs, recent research has focused on the use of natural fiber reinforcements combined with thermoplastic matrices that are heat-reformable and recyclable.[22,27–29] Natural fibers, such as flax, jute, hemp and kenaf, offer several ecological advantages, including biodegradability, low energy consumption during processing and a reduced carbon footprint compared to synthetic fibers.[30] Conversely, recent studies have shown that thermoplastic matrix composites offer superior impact resistance and faster manufacturing processes compared to traditional thermoset-based composites.[31] These properties make thermoplastics particularly advantageous in applications where durability and rapid production are critical. Additionally, thermoplastic composites can be reprocessed multiple times without significant degradation in mechanical properties, facilitating recycling and reducing environmental impact.[32] Consequently, current research is shifting toward recyclable thermoplastic matrices and natural fiber reinforcements to improve circularity and environmental performance in building composite systems.

These novel approaches not only contribute to reducing the environmental impact of composite structures but also open new opportunities for lightweight, recyclable panels in construction applications. Environmental and waste management legislations, both current and forthcoming, emphasize the need for effective recovery and recycling of engineering materials from EOL systems and materials.[33]

Despite recent advances in sustainable sandwich composites, there remains a lack of fully thermoplastic sandwich structures that simultaneously integrate renewable fiber reinforcement, lightweight design, structural performance and experimentally validated recyclability, limiting their implementation in circular construction applications.

This study hypothesizes that manufacturing both the skins and the core from the same flax-fiber-reinforced thermoplastic material enables the development of recyclable sandwich structures with mechanical performance suitable for semi-structural building applications. To test this hypothesis, a lightweight sandwich composite, termed FLACS, was designed, manufactured and experimentally evaluated using continuous flax fiber-reinforced Elium® composite for both the face sheets and the corrugated core.

The proposed architecture demonstrates the feasibility of combining renewable reinforcement, lightweight design and end-of-life recyclability within a single structural system while achieving the mechanical performance required for semi-structural applications.

These findings contribute to the development of circular composite solutions for the construction sector and support the potential use of FLACS in partition walls, ceiling panels and modular building systems.

Materials and methods

The polymer used was the liquid thermoplastic resin Elium 188 XO, with a viscosity of 100 mPa s at 25°C, purchased from Arkema (Colombes, France). The initiator was solid benzoyl peroxide (BPO) obtained from Castro Composites (Pontevedra, Spain). A mixing ratio of 3% by weight of BPO, based on the weight of resin, was employed. A 2 x 2 twill-type flax fiber fabric from Bcomp (Fribourg, Switzerland), with a weight of 200 g/m^2 and a density of 1.47 g/m^3, without surface treatment was used as reinforcement.

Preparation of composite laminates

The composite laminates with a thickness of 1.1 ± 0.03 mm were manufactured using vacuum-assisted resin infusion,[34] employing a flat glass surface as the mold. The laminates were fabricated with four fabric layers, achieving a fiber volume fraction of 50%. After mixing the resin with the hardener, it was subjected to vacuum degassing for 10 min to remove any air bubbles before the infusion. This procedure was adopted for the fabrication of the flat parts associated with the skins and the intermediate material comprising the core.

Fabrication of the core and SCSs

In the core fabrication process, the flat composite parts produced via resin infusion (Figure 2(a)) are placed into aluminum molds featuring a tile-type geometry (Figure 2(b)) to manufacture the cores by compression molding using a SATIM press (Guerlédan, France). Before molding, the flat composite part in the middle of the molds is preheated for 5 min at 200°C under no external pressure. Then, a pressure of 50 Bar is applied for 30 s. Finally, the molds are removed from the press and left to cool at room temperature for 15 min before releasing the corrugated part, Figure 2(c), to avoid polymer distortions.

The core fabrication process continues with the cutting of thin corrugated strips (Figure 2(d)) with a width equal to the required core thickness. The strips are manually joined using the same matrix system and hooks to maintain the core's shape until the desired dimension is reached, as shown in Figure 2(e). Finally, after curing at room temperature, the core is finished with sandpaper on both top and bottom surfaces to homogenize the entire thickness.

In the final manufacturing step, the honeycomb core was bonded to the laminate skins using the same polymer system employed for laminate fabrication (Figure 2(f)). To ensure adequate pressure during skin-core consolidation, the assembly was secured with clamps throughout the curing process. The specimens were then cured at room temperature, followed by post-curing at 60°C for 4 h prior to mechanical testing (Figure 2(g)).

The manual fabrication and assembly of the honeycomb core introduced dimensional variability throughout the manufacturing process, from strip cutting to the pressure applied during adhesive bonding. After the sanding and finishing stages, the parameter (c), corresponding to the strip width and ultimately defining the honeycomb core height, exhibited a final dimensional tolerance of 4.5%. However, because several

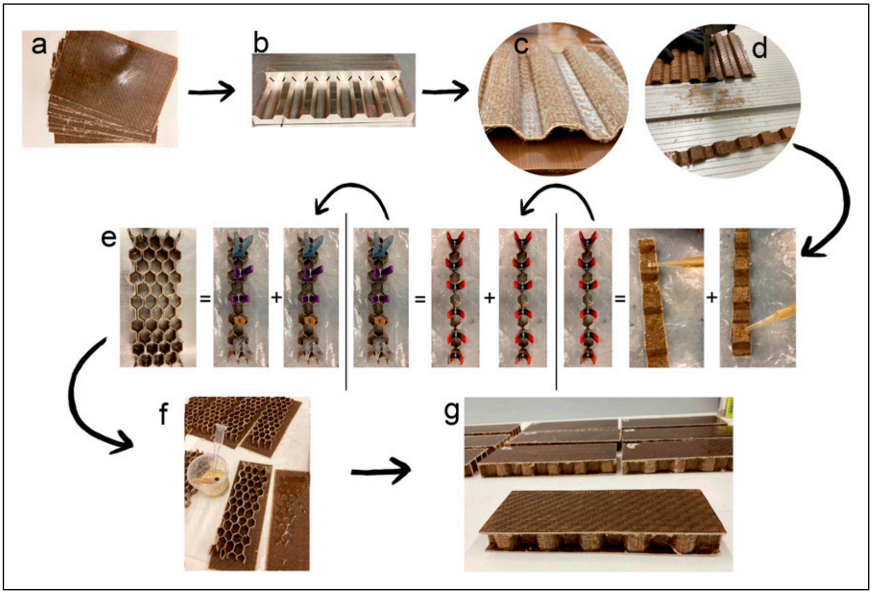

Figure 2. Sequence of core and SCS fabrication starting from the flat composite panel (a) using a corrugated mold geometry (b) the conformation of composite panels into corrugated parts after thermal compression (c) cutting the corrugated panel into strips (d) core manufacturing (e) assembly of core and skin parts (f) and the final SCS (g).

manufacturing steps depended on manual operations, minor defects were observed, such as localized skin-core interfacial gaps, which are presented and discussed in the following sections.

The geometry and dimensions of the honeycomb unit cell that comprises the core are illustrated in Figure 3 and listed in Table 1.

Single-cycle recycling of FLACS

To simulate mechanical recycling, the flat composite skin was cut into 20 × 20 mm^2 squares using an electric saw and subsequently granulated in a VESPA PA18 granulator (Pleven, Bulgaria). The shredded material (particle size <5 mm) was then hot-pressed in a SATIM press (Guerlédan, France) at 200°C for 10 min under 50 bar, followed by cooling for 200 min to produce a recycled flat composite plaque.

Determination of apparent density

In the determination of apparent density, ten samples with dimensions of (200 × 80 × 22) mm^3 were previously conditioned during 48 h at 23 ± 2°C and 50 ± 10% of relative humidity before tests, following the standard ISO 845:2006.

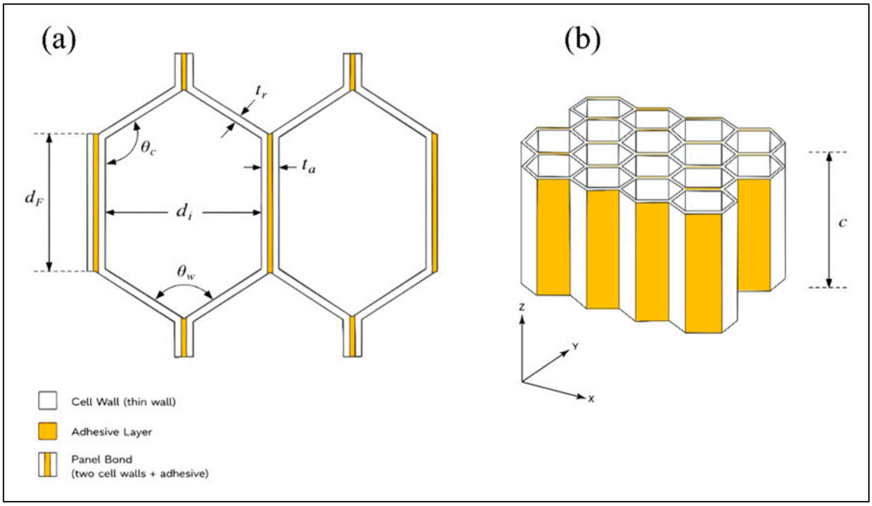

Figure 3. Geometry of the honeycomb unit cell: (a) top view and (b) isometric view of the honeycomb core.

Mechanical testing

The mechanical behavior of FLACS was determined through three-point bending, compression and impact tests, by the standards ASTM C393-22, ASTM C365-22 and ISO 6603-2:2000, respectively. The mechanical properties of the recycled and pristine composite materials were determined through a tensile test, as per ASTM D 3039. The mechanical properties were determined using five specimens for each experimental condition. However, one or two specimens exhibiting premature failure due to manufacturing defects were excluded from the final analysis. Consequently, the reported results are based on the remaining valid specimens.

A three-point bending test was conducted using a Shimadzu AG-X universal testing machine to determine the core shear properties of the FLACS. The test was performed on specimens with dimensions of 180 × 80 × 22 mm^3. A 50 kN load cell, a span length of

Table 1. Geometrical dimensions and parameters of the honeycomb unit cell.

Cell parameter	Designation	Value
Distance between inner vertical surfaces (mm)	d_i	18.4 ± 0.4
Length of adhesive bond line (mm)	d_f	12.0 ± 0.1
Cell wall thickness in the ribbon (mm)	t_r	1.7 ± 0.1
Double cell wall thickness comprising the adhesive (mm)	t_a	3.6 ± 0.2
Honeycomb core height (mm)	c	19.9 ± 0.8
Angle between ribbon and vertical walls (°)	θ_c	127.1 ± 1.3
Angle between adjacent ribbons (°)	θ_w	107.3 ± 0.8

150 mm and a testing speed of 2 mm/min were used. The force nose and supports cylinder diameters were 30 mm. The Maximum Bending Strength of the SCS (σc) in MPa, the Core Shear Ultimate Strength (τ) in MPa and the Maximum Facing Bending Strength (σf) in MPa, were calculated by equations (1)–(3) as follows:

$$\sigma c = \frac{(3Pmax)S}{2b\left(h^2 - c^2\right)} \tag{1}$$

$$\tau = \frac{3Pmax}{4bc} \tag{2}$$

$$\sigma f = \frac{(Pmax)S}{2t(h+c)b} \tag{3}$$

where,$Pmax$ = maximum force, N.h = overall SCS thickness, mm.c = core thickness, mm.b = SCS width, mm.S = span length, mm.t = face thickness, mm.

The bending modulus of elasticity of sandwich structures (D) was determined according to the procedure stablished by Brejcha et al.[35]

Specific properties (S) of the different sandwich structures were calculated taking into account both Maximum Bending Strength (σc) and bending modulus of Elasticity (D) divided by their respective density, according to the expression:

$$S\left(MPa.\,m^3.Kg^{-1}\right) = \frac{Property\,(MPa)}{Density\,(Kg.m^{-3})} \tag{4}$$

In the out-of-plane compression test, the same universal testing machine was used. A preload of 1 N was applied and the specimens were compressed between flat circular steel plates with a diameter of 200 mm. The tests were conducted at a crosshead speed of 0.5 mm/min using a 50 kN load cell. The out-of-plane compressive strength (σz) in MPa and the Compressive Modulus (Ez) in MPa of the entire sandwich structures were calculated by equations (5) and (6), as follows:

$$\sigma z = \frac{Pmax}{A} \tag{5}$$

$$Ez = \frac{\Delta\sigma}{\Delta\varepsilon} \tag{6}$$

where,$Pmax$ = maximum peak force, N.A = cross-sectional area, mm^2.$\Delta\sigma$ = stress change within the linear elastic region. $\Delta\varepsilon$ = strain change within the linear elastic region.

A CEAST 9350-Fractovis Plus impact-testing machine was used to determine the impact resistance of FLACS using a hemispheric dart of 20 mm in diameter. Samples with dimensions of (80 × 80 × 22) mm^3 were impacted in a closed chamber at a speed of 4.4 m/s with a mass of 10 Kg from a height of 1 m, corresponding to an approximate energy of 98 J. Values for maximum force and energy absorption were recorded.

Tensile tests were carried out using an Instron 5969 machine equipped with a 50 kN load cell and a video strain gauge. The speed of testing was set to 2 mm/min. The maximum tensile strength and the strength at the point of failure were recorded.

Fracture analysis

A FEI NOVA 200 ultra-high-resolution scanning electron microscope (FEG/SEM) was used in secondary electron (SE) mode at a power of 10 kV to perform a fractographic analysis of the 3-point bending specimens and determine the fracture characteristics. A thin layer of gold was applied to each surface to enhance the sample's conductivity.

Results

The calculated apparent density of the core developed in this study, in comparison to other commercial alternatives for core materials, is presented in Table 2.

As shown in Table 1, the apparent density of the Flax/Acrylic core falls within the typical range reported for core materials employed in sandwich-structured composites. It is important to highlight that, although the densities of polyurethane (PU) and polystyrene (EPS) foams may be lower than that of the developed cellular core, these materials present significant limitations in terms of recyclability and potential for reuse in new applications. In the case of PU, post-curing cross-linking hinders depolymerization into initial monomers and restricts thermal processability. For EPS, the volatility of its constituent particles and its low density make its recycling both technically and economically unfeasible. Conversely, aluminum and aramid honeycomb cores exhibit a broad and versatile density range, influenced by factors such as cell size, cell count per unit volume and cell wall thickness.

Nevertheless, aramid cores present environmental concerns due to their composition, which typically includes phenolic resins.[36,37] In contrast, although the core developed in this study is of the hexagonal type, it features a single cell size and wall thickness, both of which are determined by the available mold and manufacturing process. The calculated

Table 2. Densities of different core materials.[36–41]

Material	Density (Kg/m^3)
Flax/Acrylic[a]	125 ± 12
Hexagonal aluminum	26-610
Kraft paper honeycomb	23-56
Nomex honeycomb	24-200
Polystyrene foam	56-70
Balsa wood	96-250
Stainless steel honeycomb	120-150
Polyurethane foam	42-120
Cork honeycomb	74-146

[a]Indicates the core material developed in this study.

density of the FLACS was 234 ± 12 kg/m^3, a value that accounts for both the core and the two faces of the sandwich composite structure. The density of the flat composite faces was measured at 1240 ± 20 kg/m^3, with an estimated void content of 4.5 ± 0.6%.

Based on this information, the theoretical density of the composites constituting the skins can be calculated using the rule of mixtures,[38] assuming a constant fiber volume fraction of 0.5 and the absence of voids within the laminate. These values, along with those of other composites fabricated with the same resin system but different reinforcement phases, are presented in Table 3.

In this regard, the manufactured composite demonstrates a clear advantage in terms of density when compared to laminated composites reinforced with other industrial-grade fibers. Consequently, the overall density of the sandwich composite structure will increase proportionally with the mass of the face sheets, implying that for denser laminates, the use of lighter cores becomes essential to balance the total mass of the structural element.

During the assembly of the skins to the honeycomb core, localized skin–core interfacial gaps were observed, despite the cores being sanded and dimensionally finished before assembly and secured with clamps during adhesive curing (Figure 4).

The lack of adhesion between the core and the face sheets occurs in some areas of the structure, primarily due to the heterogeneity in the height of the fabricated core along its bonding line. This limitation, resulting from the manual fabrication of each core element, could be mitigated using automated surface finishing machines, which would enable stricter dimensional control.

Bending test

The load-displacement curves from Figure 5 indicate that the fabricated panels exhibit heterogeneity, which is directly related to the core manufacturing process and its subsequent bonding to the face sheets of the sandwich composite structure, both of which are carried out manually. This heterogeneity influences their failure mechanisms.

Nevertheless, it can be inferred that during the initial loading phase, the panels undergo a stage in which all phases act synergistically, with effective load transfer occurring among the constituent elements of the panel. This load transfer persists up to the maximum peak load, after which a first drop in load is observed. This drop is

Table 3. Theoretical densities of composite laminates comprising the skins, for V_f = 0.5 and resin density of 1.15 g/cm^3, according to the resin manufacturer.

Fiber type	Fiber density (g/cm^3)	Composite density (g/cm^3)
Flax[a]	1.47	1.31
Glass	2.60	1.88
Carbon	1.78	1.47
Aramid	1.45	1.30
Basalt	2.70	1.93

[a]Materials constituting the composite laminate skins of this study.

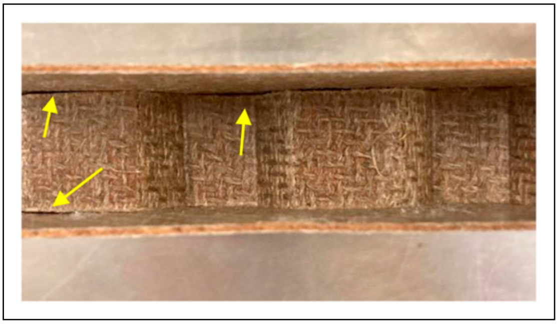

Figure 4. FLACS presenting poor adhesion between the core and skins.

associated with the detachment of the top face sheet, caused by shear forces acting at the skin-core interface. In cases where skin-core adhesion is poor, continued load bearing becomes unfeasible, leading to catastrophic failure of the panel, as evidenced by the curve for sample 1. For the remaining curves, despite an initial local skin-core debonding, the elements continue to carry load at higher strain levels, indicating greater damage tolerance. The stepwise force drops observed in curves 2 to 4 are indicative of progressive delamination within the material, which can suggest progressive fiber breakage produced

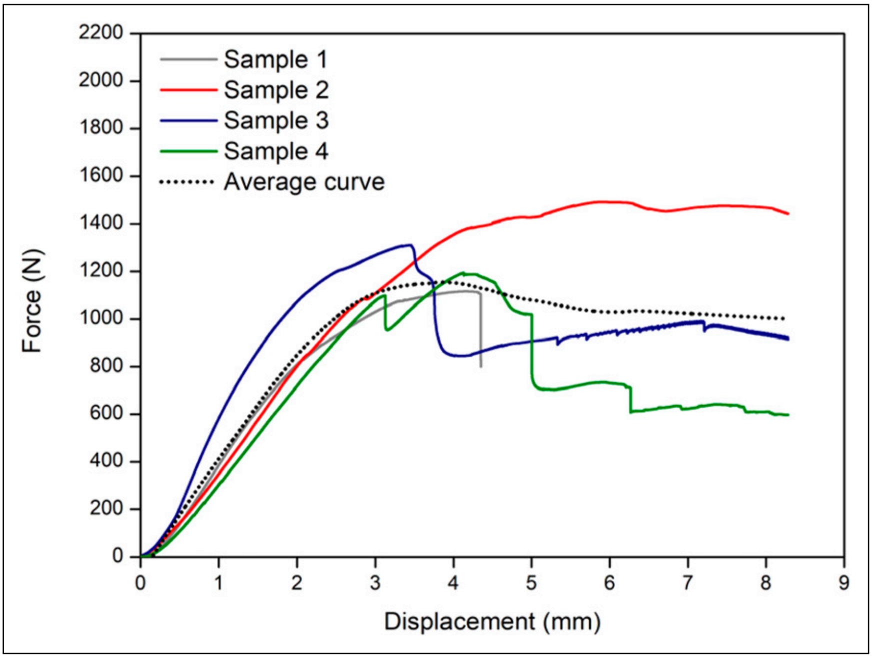

Figure 5. Force vs displacement curves for FLACS tested in 3-point bending. The dotted line indicates the average curve.

by the combination of compression and tensile stresses. The values related to the bending properties of FLACS are presented in Table 4.

The flexural properties of the FLACS structures were compared with those of other structures reported in the scientific literature, as shown in Table 5, allowing for the identification of the advantages and limitations of the structures developed in the present study. In terms of maximum load-bearing capacity and structural stiffness, FLACS exhibits superior values, indicating that the thin-walled hexagonal core structure reduces the tendency for collapse under low load levels due to its higher buckling resistance. It is worth noting that although cork-based hexagonal structures[39] also present a hexagonal geometry, the continuous fibers in the FLACS core provide a more uniform and efficient load distribution. In this context, flax fiber is considered continuous since its length was not reduced prior to its incorporation into the matrix, and its length greatly exceeds the critical fiber length, thus suggesting that load transfer occurs and is superior to that of the unreinforced matrix.

The maximum flexural strength shows values that are 36% lower than those reported for GF-EPX/Cork NL20, suggesting that this system exhibits greater adhesion between the faces and the core. It also explains the shear strength values obtained, indicating greater resistance to face-to-face sliding, which also reduces core deformation at low load levels. The high stiffness of glass fibers and their strong adhesion with epoxy systems also elucidate the superior efficiency of this type of structure when compared to the systems proposed in this study. As observed, FLACS exhibited 180% higher specific strength (Sp.σc) than GF-EPX/Cork NL20 and the various combinations of flax-epoxy-based sandwich structures. In terms of specific modulus (Sp.D), this trend maintains, with FLACS presenting twice the specific modulus of GF-EPX/PVC foam structures. This behavior could also be attributed to the type of material used in the core and its cellular structure, which, in the case of FLACS, has a void fraction of approximately 75%. In contrast, for PU and thermoplastic foams, the air content typically exceeds 90%,[43] whereas for aluminum or aramid honeycombs, the values exceed 85%. The core used in the FLACS structure is composed of approximately 25% solid material, which forms the cell walls and provides structural integrity to the core, preventing premature deformation under initial mechanical loading.

Although all geometric parameters of the honeycomb unit cell exhibited some degree of dimensional variability as a consequence of the non-automated manufacturing process, the observed variations in the core height (c) are expected to have the greatest influence on the bending response. The manual bonding process also introduced localized skin-core defects, including small interfacial, which reduced shear-transfer efficiency and

Table 4. Mechanical properties of FLACS from three-point bending test.

Property	Average value	SD
P_{max} (N)	1178	164
σc (MPa)	41	4
τ (MPa)	0.6	0.06
σf (MPa)	27.3	2.8
D (MPa)	5800	700

Table 5. Flexural properties of FLACS (underline) in comparison to similar works found in the literature.[25,35,39,40,42]

Material	P_{max} (*N*)	**σc** (MPa)	τ (MPa)	D (MPa)	**σf** (MPa)	Density (Kg/m^3)	Sp. **σc** (MPa·m^3/kg)	Sp. **D** (MPa·m^3/kg)
FLACS	1178	41	0.6	5800	27.3	234	0.18	24.8
GF-EPX/ Cork	829	—	0.1	—	10	297	—	—
GF-EPX/ Cork NL20	—	56	0.9	4000	—	560	0.10	7.1
EPX-PES knitted fabrics	70	—	0.2	—	2.5	—	—	
FF-EPX/ Bamboo	—	11.6	0.9	4200	49	390	0.03	10.8
GF-EPX/PVC foam	1150	43.9		5100		417	0.11	12.2
FF-EPX/PVC foam	780	38.4		2400		432	0.09	5.6
FF-EPX/Balsa	600	30.8		2400		405	0.08	5.9

GF: glass fibers; EPX: epoxy resin; PES: polyester; FF: flax fibers.

promoted premature interfacial failure. Although the influence of core height was not investigated as an independent variable in this study, the experimental observations, supported by classical sandwich structural mechanics, suggest that tighter control of core height and skin-core consolidation would improve the repeatability and mechanical performance of manually manufactured sandwich panels.

As shown in Table 5, FLACS does not necessarily outperform all the reference sandwich structures in terms of absolute flexural properties. Its main advantage emerges when mechanical performance is normalized by density, resulting in higher specific strength and stiffness than the compared systems. This finding indicates that the benefit of FLACS lies primarily in its mechanical efficiency at low weight rather than in maximizing absolute strength. The results therefore suggest a favorable trade-off between structural performance and material weight, which is particularly relevant for lightweight building applications.

An analysis was conducted to determine the fracture characteristics of the composite after being subjected to three-point bending tests. Figure 6 shows the loading condition and its effects on the integrity of the sandwich panel. The upper face, in contact with the loading nose and subjected to compressive forces, exhibits significant plastic deformation (Figure 6(a) and (b)), resulting in a permanent indentation of the skin that promotes its separation from the core. This plastic behavior correlates with the ductility observed in the force-displacement curves.

Additional signs of face-core debonding at the lower face of the structure, caused by shear forces acting along the core-face adhesive interface, were also observed in

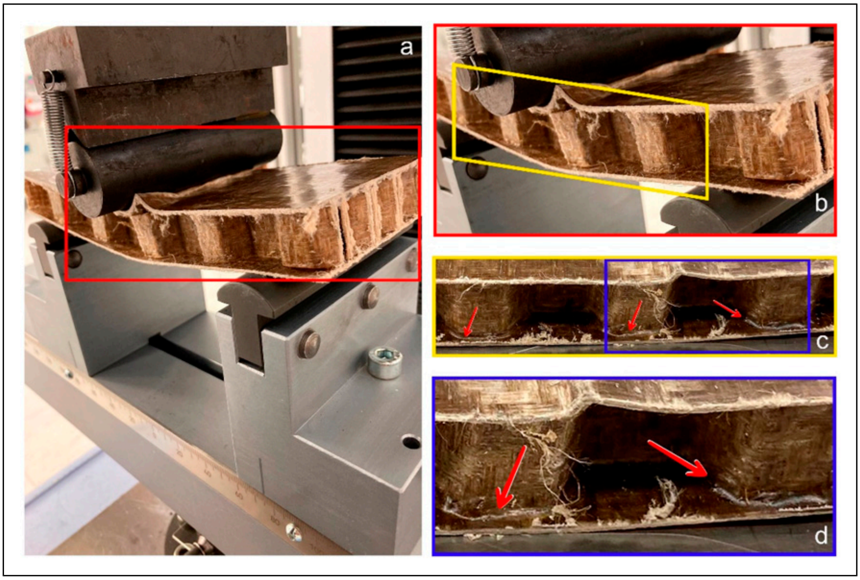

Figure 6. FLACS during the three-point bending test displaying the test setup (a) skin deformation in the upper face (b) and core debonding with the lower face (c) and (d) indicated with red arrows.

Figure 6(c) and (d), and are indicated by red arrows. The core itself did not show collapse or visible damage in any of the tested panels, with the front and rear faces of the FLACS structures being the most affected components during the three-point bending tests.

Figure 7(a) shows the wrinkle generated by compressive loads on the front face of the FLACS structure, which confirms the plastic deformation capability of the manufactured composite. It also reveals the presence of fibers without matrix residue that were exposed during the cutting of the panel. Figure 7(b) shows 45° cracks observed on the surface of the face, which may suggest shear stresses produced during the rotation of the fracture surface. These bands are accompanied by surface irregularities associated with polymer fracture, which occurs due to surface thinning where cracks initiate and coalesce. Additionally, residual porosity is observed, related to the mold surface where the skins were produced. Figure 7(c) highlights loose, non-impregnated fibers that were pulled out during panel cutting, while fibers embedded in the polymer matrix are visible in the background. On the surface of the skin, cracks aligned parallel to the fiber direction are observed, which may suggest fiber-matrix detachment (red arrows).

Figure 7(d) shows the rear face of the composite, where tensile stresses are present. Transverse cracks, as well as others parallel to the fiber direction, are visible, resulting in delamination and material failure in the central region of the face. Figure 7(e) shows fiber breakage, fiber pull-out and fiber misalignment, the latter induced by high matrix deformation. Fibers impregnated with the matrix are also observed, as their surfaces do not exhibit the characteristic roughness of untreated fibers.[30,44] However, these fibers are detached, suggesting matrix debonding and possible cohesive failure. Figure 7(f) also

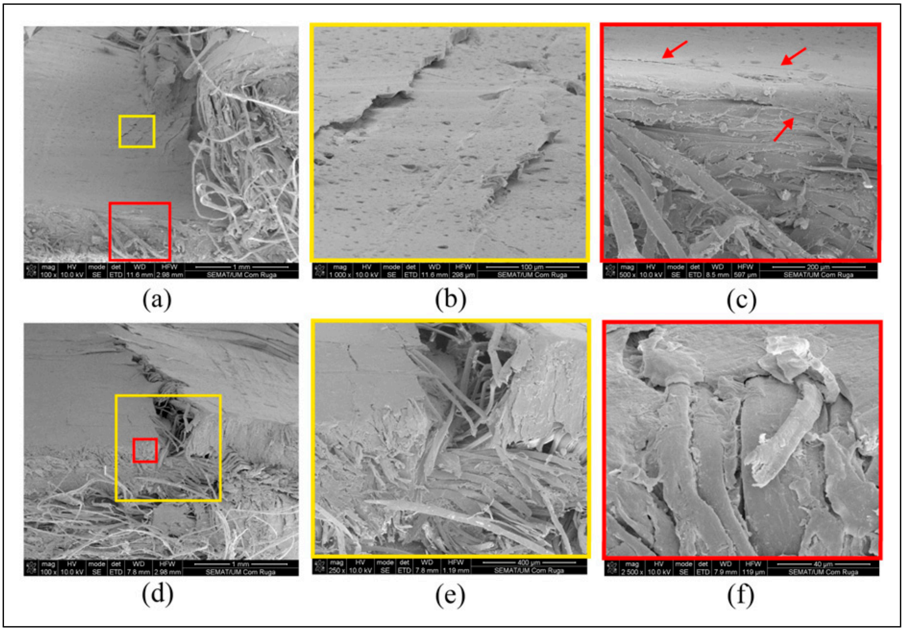

Figure 7. SEM micrographs showing the fracture surfaces of the top and bottom skins of the FLACS. Micrographs (b) and (c) provide higher-magnification views of the areas highlighted in micrograph (a), following the color code. Likewise, micrographs (e) and (f) display enlarged details of the regions marked in micrograph (d) using the same color reference.

shows fibers well bonded to the matrix with a smooth surface appearance, which may confirm that the fibers are impregnated and maintain interfacial integrity under the tensile stress level supported by the skin.

Out-of-plane compression

Through the analysis of the stress–strain curve shown in Figure 8, it is possible to identify three distinct zones representing the material's behavior. The first zone is characterized by a linear increase in stress, corresponding to an elastic region with lower stiffness (zone I), which is related to the coupling between the core and the faces of the structure. In this specific case, voids along the bonding line, caused by curvature effects or misalignment, result in reduced resistance to deformation under low load levels. Once all elements in the structure become fully engaged, the stress increases linearly, defining the elastic region (zone II) up to the maximum stress sustained before the onset of permanent deformation. Within this region, the material undergoes no significant dimensional changes upon unloading.

After yielding occurs, a slight drop in stress, known as post-yield softening,[45] is followed by an almost constant stress region, zone III (stress plateau), where the collapse of the core cells begins. This region defines the plastic deformation of the FLACS

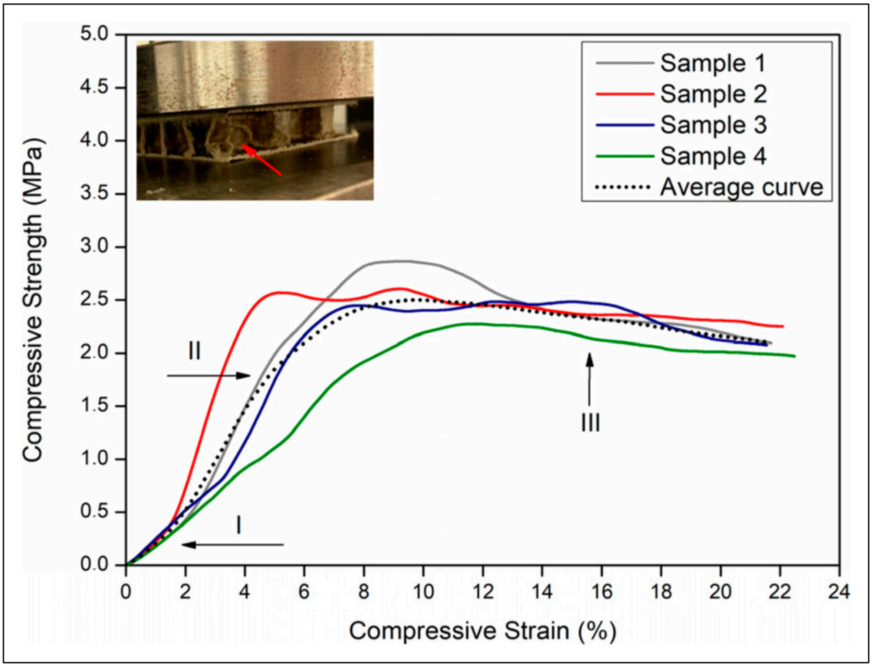

Figure 8. Out-of-plane compression curves for FLACS with a dotted line indicating the average curve. The inset in the figure displays the core collapse during the compressive test.

structure, in which a nearly constant stress is observed as deformation increases. This plateau determines the energy absorption capacity of the sandwich structure.[46] The deformation of the cell walls occurs collectively; that is, the adhesion between the cell walls is sufficient for them to deform together without separation. Additionally, during the compression test, it was observed that the outer walls of the core exhibited buckling followed by progressive collapse (inset, Figure 8). In the cases studied, no densification region, commonly seen in cellular solids, was observed.[47]

The scatter observed in the out-of-plane compressive response can be attributed, at least in part, to the dimensional variability introduced during the manual manufacturing process. Localized skin-core defects, including non-uniform adhesive thickness, likely reduced load-transfer efficiency, promoting premature failure under compression. The results of the compression tests on the FLACS structures are summarized in Table 6.

The out-of-plane compressive modulus (99.4 MPa) was considerably lower than the flexural modulus (5.8 GPa). This difference is expected because the two tests evaluate different structural mechanisms. During bending, the composite face sheets carry most of the tensile and compressive stresses, while the honeycomb core mainly maintains the separation between the skins and transfers shear loads, resulting in a high flexural stiffness. Conversely, under flatwise compression, the deformation is governed primarily by the honeycomb core, together with the adhesive interfaces, where localized cell-wall bending, buckling and progressive crushing occur. Consequently, the out-of-plane

Table 6. Out-of-plane compression properties of FLACS.

Property	Average value	SD
P_{max} (kN)	19.6	2.0
σz (MPa)	2.4	0.2
Ez (MPa)	99.4	12.7

compressive modulus is substantially lower than the flexural modulus, despite both properties being measured on the same sandwich structure.[48] The out-of-plane compressive strength of FLACS (2.4 ± 0.2 MPa) is comparable to values reported for other lightweight thermoplastic sandwich structures based on natural fibers. For instance, flax/PLA sandwich panels with PLA honeycomb cores exhibited flatwise compressive strengths ranging from 1.7 to 2.6 MPa, depending on the core thickness.[49] In contrast, higher compressive strengths of approximately 13.5–15.5 MPa have been reported for jute/vinylester honeycomb cores.[50] However, these higher values were associated with relatively dense cores and comparatively thick cell walls and their specific compressive strengths were reported to be comparable to those of commercial honeycomb cores. Therefore, the compressive performance of FLACS should be considered in conjunction with its particularly low density (234 kg/m^3) rather than solely in terms of absolute strength. From this perspective, the obtained compressive properties, together with the thermoplastic nature and mechanical recyclability of the proposed structure, indicate a favorable compromise between lightweight performance, load-bearing capability and end-of-life recyclability.

Impact properties

The force versus time curves of the tested samples is presented in Figure 9(a). The curves exhibit two main force peaks, which are associated with the resistance of the material faces to penetration by the impact dart. In the first force peak, occurring between 2 and 4 ms, the front face of the structure, initially exposed to the impact, experiences a force of approximately 1300 N, indicating the high resistance of the material to being impacted and subsequently penetrated by the dart. However, the force then drops to values around 150 N due to the core structure, which acts as a structural support and alters the trajectory of the dart.

In this initial force peak, the material exhibits combined resistance to dart penetration, with both the face and the core structure absorbing and distributing part of the impact energy, resulting in high load peaks. The second force peak, observed between 7 and 9 ms, corresponds to the impact and penetration of the rear face of the structure, reaching forces of approximately 400 N. The reduction in the force supported by the rear face, compared to the front face, is attributed to the absence of the core as a supporting or energy-dissipating structure during this phase of the impact. Subsequently, the force curve drops to minimal values, indicating the complete perforation of the structure (Figure 9(b)), which is consistent with the maximum displacement obtained. The impact properties of FLACS are summarized in Table 7.

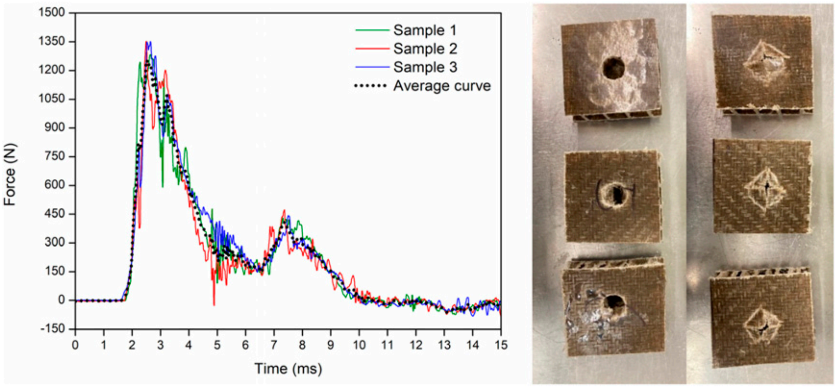

Figure 9. (a) Impact resistance curves of FLACS, with the dotted line representing the average response; (b) photographs of the impacted specimens showing the top (left) and bottom (right) faces.

The impact response of FLACS was further contextualized through comparison with natural-fiber sandwich structures reported in the literature. Flax-based sandwich composites incorporating different lightweight cores, including agglomerated cork, balsa and polymeric honeycomb structures, have demonstrated their ability to dissipate energy under low-velocity impact loading.[51,52] Sandwich panels combining flax-FRP faces with polymeric foam cores have also shown resilient behavior after repeated impact events.[53] FLACS exhibited a maximum impact force of 1.28 ± 0.03 kN and an absorbed energy of 14.07 ± 0.6 J under an incident energy of 98 J. Direct quantitative comparison with previously reported sandwich structures is limited by differences in material configurations and testing conditions. Nevertheless, the impact performance of FLACS, together with its lightweight design and mechanical recyclability, highlights its potential for sustainable building applications.

Tensile properties of the recycled material

For the recycling process, a flat composite panel representative of the FLACS structure was selected. In this configuration, both the skins and the core were manufactured from

Table 7. Impact properties of FLACS.

Property	Average value	SD
Maximum force (*N*)	1280	32.2
Displacement at maximum force (mm)	3.86	0.6
Maximum displacement (mm)	34.90	1.4
Absorbed energy (J)	14.07	0.6

the same laminate, without the use of adhesives or reinforcements of a different nature. This homogeneous material composition ensures the complete recyclability of the sandwich structure developed in this study.

For practical and demonstrative purposes, a flat-panel geometry was selected to facilitate the cutting and subsequent granulation processes. The resulting granulated material, with a recovery yield of 95% (Figure 10(a)), was subsequently sieved using a series of standard sieves to determine its particle size distribution, as presented in Figure 10(b). Then, a flat plaque of the recycled composite (Figure 10(c)) was produced according to the procedure described in the materials and methods section.

The particle size distribution obtained after granulation deserves several considerations. First, the particle sizes determined by sieve analysis generally correspond to fiber-matrix fragments, in which the flax fibers remain embedded within the PMMA matrix. Consequently, the actual fiber lengths are expected to be shorter than the measured particle dimensions. Furthermore, the granulation process produced a predominance of fine particles, with 74% of the material exhibiting characteristic dimensions below 2.0 mm, 12% falling within the 2.0–3.4 mm interval and only approximately 15% exhibiting particle dimensions greater than 3.4 mm.

Table 8 presents the mechanical properties resulting of the recycling of the structure in comparison with the original material processed by resin infusion.

As expected, the composite material subjected to mechanical recycling followed by thermo-mechanical processing exhibited a reduction in its mechanical properties, with decreases of 62%, 31% and 62% in ultimate tensile strength, elastic modulus and elongation at break, respectively. It is mainly attributed to the reduction in fiber length, which approaches values below the critical fiber length.[54] For flax fibers with diameters between 70 and 90 μm and a tensile strength between 1500 MPa,[43] the critical fiber length (L_c) ranges between 2.6 and 3.4 mm. L_c was determined using an interfacial shear strength of 21 MPa for untreated flax fibers embedded in an Elium matrix.[55]

Considering that the critical fiber length is within the range of 2.0–3.4 mm, only 12% of the particles fell within this interval, while approximately 15% exceeded the critical fiber length. These results indicate that most of the recycled reinforcement is likely composed of fibers shorter than or close to the critical length, which limits the efficiency of stress transfer from the matrix to the fibers. As a result, the reinforcing capability of the

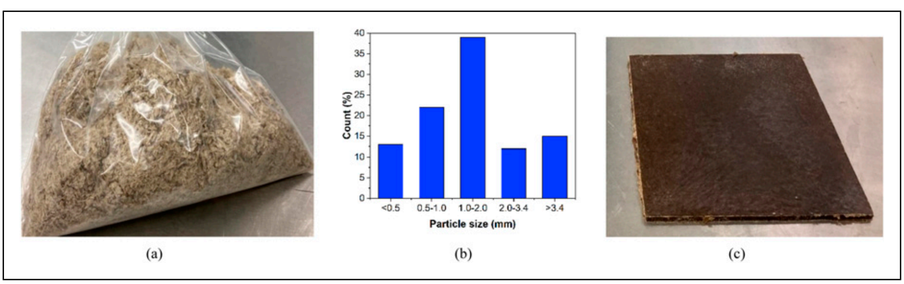

Figure 10. Recycled FLACS material showing (a) ground particles, (b) particle size distribution after sieving, and (c) the laminate produced by thermo-mechanical compression molding.

Table 8. Tensile properties of composites for the original and recycled conditions.

Property	Original composite	Recycled composite
σ_{max} (MPa)	90.0 ± 8.6	34.4 ± 2.1
E (GPa)	5.8 ± 0.6	4.0 ± 0.3
ε_{max} (%)	3.4 ± 0.1	1.3 ± 0.2

recycled material is expected to be significantly reduced compared with that of the original continuous-fiber laminate.

Furthermore, because a considerable fraction of the recycled fibers is expected to be shorter than the critical length, these fibers are more likely to behave as discontinuities than as effective load-bearing reinforcements. This behavior contributes to stress concentration within the composite, providing a plausible explanation for the reduction in tensile strength and failure strain observed in the recycled material. To minimize the loss of mechanical properties, future work should investigate alternative granulation conditions, including the use of screens with larger mesh openings and lower cutting speeds, as well as alternative size-reduction methods capable of preserving recycled particles larger than L_c. It should be noted that a technically viable recycling process should preferably minimize material losses. Therefore, the selective use of recycled particles based on their size, involving the exclusion of finer fractions, would not be considered a practical or sustainable approach.

Similar trends have been reported for mechanically recycled flax-fiber thermoplastic composites, where the reduction in tensile strength has been mainly attributed to fiber shortening during size reduction and the resulting loss of reinforcement efficiency.[56] For flax/Elium composites recycled by thermocompression, tensile strengths of approximately 15.6 MPa and moduli around 5.4 GPa have been reported after the first recycling cycle, with further recycling causing additional changes in the mechanical response.[57] In flax/MAPP composites, mechanical recycling has been reported to reduce mechanical properties by up to approximately 75% relative to the original continuous-fiber material.[58] Within this context, the recycled FLACS composite shows a comparatively favorable retention of stiffness after a single recycling cycle. Moreover, the approximately 95% recycling yield achieved in the present process indicates that this mechanical recycling route can recover most of the original material while producing a second-generation composite with useful mechanical properties.

In the presented work, the residual polymer retained after the recycling process was sufficient to promote particle consolidation without the addition of a new polymeric phase. Nevertheless, the recycled laminate was approximately 6.4% lighter than the original laminate and exhibited surface defects, including waviness and fiber print-through, indicative of matrix shrinkage, Figure 10(c). These defects were more pronounced in the recycled laminate due to the limited control of the cooling process and the random orientation and distribution of the short reinforcement phase, which is less effective than the original continuous fiber architecture at restraining polymer shrinkage during cooling.

The recycling process investigated in this study was limited to a single thermo-mechanical recycling cycle. The end-of-life composite was mechanically granulated and subsequently reprocessed by hot compression molding. During this stage, the residual PMMA matrix was softened/remelted, enabling particle consolidation without the addition of virgin polymer or any chemical treatment. No depolymerization or chemical recycling step was involved. Consequently, the process relies exclusively on the thermoplastic nature of the PMMA matrix to achieve material reprocessing and particle consolidation. Although the results demonstrate the feasibility of recovering FLACS through a single recycling cycle, further studies are required to assess the effects of multiple recycling cycles on the material's long-term mechanical performance and recyclability. The sandwich-type composite structure presented here exhibits clear advantages in specific strength and recyclability compared with other materials and similar structures reported in the literature. However, it is worth noting that the stepwise manufacturing route used in this exploratory stage of development should be refined to avoid sample variability arising from manual procedures and the associated defects in the assembly process of the structural components.

One of the principal limitations of the manufacturing process proposed in this work is the cutting of the corrugated strips that constitute the composite core. The current cutting procedure results in variations in the final core height, leading to inadequate and non-uniform contact between the core and the sandwich skins during assembly. These dimensional inconsistencies compromise the quality of the bonded interface and increase the likelihood of premature interfacial failure, ultimately reducing the structural efficiency and reliability of the sandwich composite. Addressing this limitation is therefore essential to improve both the mechanical performance and the repeatability of the manufacturing process. The implementation of more precise cutting technologies, such as laser cutting, waterjet cutting, high-precision CNC machining or other digitally controlled cutting methods, is recommended to achieve tighter dimensional tolerances and ensure greater consistency in the geometry of the core elements.

Further improvements can also be achieved by optimizing the core-to-skin bonding process. The incorporation of robot-assisted assembly systems, combined with thermal fusion techniques or the application of high-performance structural adhesives, would enable a higher degree of process standardization while minimizing operator-dependent variability. Such approaches are expected to reduce interfacial defects and enhance the overall scalability of the process for industrial production.

In addition to manufacturing optimization, further experimental investigations are recommended to evaluate the suitability of the developed structures for practical construction and architectural applications. Specifically, compatibility with conventional mechanical fastening systems should be assessed to determine the feasibility of integrating the panels into existing construction practices. Likewise, the adhesion and compatibility of the composite surfaces with commonly used finishing materials (plasters, primers and protective coatings) should be investigated to ensure adequate performance during installation and service. Finally, a comprehensive characterization of the thermal and acoustic insulation properties of the sandwich structures is necessary, as these functional attributes are critical for assessing their potential as multifunctional building components capable of providing both structural performance and enhanced environmental comfort.

Therefore, this work presents a promising development path that can be further refined through complementary studies, thereby providing an alternative approach for the design of lightweight semi-structural components, including partition walls, ceiling panels and modular building. Moreover, it opens the possibility for these structures, upon the end of their service life, to be reintroduced into new manufacturing processes, thereby enhancing the sector's circularity.

Conclusions

In this work, a sandwich-type composite structure (FLACS) with a honeycomb core and flax fiber-PMMA skins was developed, using vacuum infusion for the skins, a combination of vacuum infusion and compression molding for the core and manual assembly to join the components.

FLACS exhibited a low density of 234 kg/m^3, considerably lower than that of comparable sandwich structures reported in the literature. Mechanical characterization demonstrated a maximum flexural strength of 41 MPa, a core shear strength of 0.6 MPa, a face stress of 27.3 MPa and a flexural modulus of 5.8 GPa. Under compression, FLACS reached a compressive strength of 2.4 MPa and a compressive modulus of 99.4 MPa, while low-velocity impact tests showed an energy absorption of up to 14 J. Particularly noteworthy are the specific strength and specific modulus of 0.18 and 24.8 MPa·m^3/kg, respectively, highlighting the lightweight performance of the proposed structure.

The results also demonstrate the importance of manufacturing quality in achieving consistent mechanical performance. Although the panels were produced using predominantly manual manufacturing procedures, further improvements are expected through enhanced process control and the implementation of automated cutting, assembly and bonding operations, enabling greater reproducibility and reducing manufacturing-induced variability.

A further advantage of the proposed material is its recyclability. The panels were successfully recycled through a single mechanical recycling cycle with a recycling yield of approximately 95%, demonstrating a significant benefit over conventional thermoset-based sandwich composites. Although a reduction in mechanical performance was observed after recycling due to fiber shortening during the granulation process, future optimization of the size-reduction conditions, offers a practical route to improve the mechanical performance of the recycled material while maintaining a technically viable process with minimal material losses.

Overall, the combination of specific mechanical properties, impact resistance and recyclability establishes FLACS as a promising lightweight and sustainable sandwich structure for future building applications.

Acknowledgments

The authors acknowledge the Institute for Polymers and Composites – IPC and the Laboratory for Materials Characterization Services – SEMAT of the University of Minho for their important support to carry out this research. Authors also acknowledge the Center for Innovation in Polymer Engineering – PIEP.

ORCID iD

Braian Uribe https://orcid.org/0000-0002-7229-0874

Author contributions

B.U. contributed to conceptualization, methodology, investigation, writing—editing; R.P. carried out formal investigation and writing of the original draft; P.A. helped in methodology, data curation, formal analysis and writing; B.U. and P.A. helped in financial support. All authors have read and agreed to the published version of the manuscript.

Funding

The authors disclosed receipt of the following financial support for the research, authorship, and/or publication of this article: This research was funded by the Fundação para a Ciência e Tecnologia—FCT with funding through the National Funds Reference, grant number UID/05256/2025 Institute for Polymers and Composites, University of Minho.

Declaration of conflicting interests

The authors declared no potential conflicts of interest with respect to the research, authorship, and/or publication of this article.

Data Availability Statement

The original contributions presented in this study are included in the article. Further inquiries can be directed to the corresponding author.

References

1. Kausar A, Ahmad I, Rakha SA, et al. State-of-the-art of sandwich composite structures: manufacturing—to—high performance applications. *J Compos Sci* 2023; 7(3): 102. https://doi.org/10.3390/jcs7030102, Epub ahead of print 2023.
2. George T, Deshpande VS, Sharp K, et al. Hybrid core carbon fiber composite sandwich panels: fabrication and mechanical response. *Compos Struct* 2014; 108: 696–710. https://doi.org/10.1016/j.compstruct.2013.10.002
3. He M and Hu W. A study on composite honeycomb sandwich panel structure. *Mater Des* 2008; 29: 709–713. https://doi.org/10.1016/j.matdes.2007.03.003
4. Zhao T, Yang J, Chen J, et al. Review of carbon fiber-reinforced sandwich structures. *Polym Polym Compos* 2022; 30: 09673911221098729. https://doi.org/10.1177/09673911221098729
5. Choi Y, Kang W, Moon J, et al. Optimum design of sandwich composite structures under various dynamic loads using the equivalent static load method. *Compos Struct* 2022; 298: 115991. https://doi.org/10.1016/j.compstruct.2022.115991
6. Njim EK, Hasan HR, Jweeg MJ, et al. Mechanical properties of sandwiched construction with composite and hybrid core structure. *Adv Polym Technol* 2024; 2024: 3803199. https://doi.org/10.1155/2024/3803199

7. Manalo A, Aravinthan T, Fam A, et al. State-of-the-art review on FRP sandwich systems for lightweight civil infrastructure. *J Compos Construct* 2017; 21: 4016068. https://doi.org/10.1061/(asce)cc.1943-5614.0000729
8. Siriruk A, Jack Weitsman Y and Penumadu D. Polymeric foams and sandwich composites: material properties, environmental effects, and shear-lag modeling. *Compos Sci Technol* 2009; 69: 814–820. https://doi.org/10.1016/j.compscitech.2008.02.034
9. Palomba G, Gabriella E and Crupi V. Lightweight sandwich structures for marine applications: a review. *Mech Adv Mater Struct* 2022; 29: 4839–4864. https://doi.org/10.1080/15376494.2021.1941448
10. Patekar V and Kale K. State of the art review on mechanical properties of sandwich composite structures. *Polym Compos* 2022; 43: 5820–5830. https://doi.org/10.1002/pc.26989
11. Dariushi S and Sadighi M. A study on flexural properties of sandwich structures with fiber/metal laminate face sheets. *Appl Compos Mater* 2013; 20: 839–855. https://doi.org/10.1007/s10443-012-9307-2
12. Van Voorhees EJ and Green DJ. Mechanical behavior of a ceramic sandwich composite system. *J Compos Mater* 1992; 26: 1664–1677. https://doi.org/10.1177/002199839202601106
13. Chen Y and Das R. A review on manufacture of polymeric foam cores for sandwich structures of complex shape in automotive applications. *J Sandw Struct Mater* 2022; 24: 789–819. https://doi.org/10.1177/10996362211030564
14. Khan T, Acar V, Aydin MR, et al. A review on recent advances in sandwich structures based on polyurethane foam cores. *Polym Compos* 2020; 41: 2355–2400. https://doi.org/10.1002/pc.25543
15. Tripathi L and Behera BK. Comparative analysis of aluminium core honeycomb with 3D woven Kevlar honeycomb composite. *Mater Sci Technol* 2023; 39: 1697–1708. https://doi.org/10.1080/02670836.2023.2180601
16. Mugahed Amran YH, El-Zeadani M, Huei LY, et al. Design innovation, efficiency and applications of structural insulated panels: a review. *Structures* 2020; 27: 1358–1379. https://doi.org/10.1016/j.istruc.2020.07.044
17. Boafo FE, Kim J-H and Kim J-T. Performance of modular prefabricated architecture: case study-based review and future pathways. *Sustainability* 2016; 8(6): 558. https://doi.org/10.3390/su8060558, Epub ahead of print 2016.
18. Sah TP, Lacey AW, Hao H, et al. Prefabricated concrete sandwich and other lightweight wall panels for sustainable building construction: state-of-the-art review. *J Build Eng* 2024; 89: 109391. https://doi.org/10.1016/j.jobe.2024.109391
19. Post W, Susa A, Blaauw R, et al. A review on the potential and limitations of recyclable thermosets for structural applications. *Polym Rev* 2020; 60: 359–388. https://doi.org/10.1080/15583724.2019.1673406
20. Farrelly TA and Shaw IC. Polystyrene as hazardous household waste. In: Mmereki D (ed). *Household hazardous waste management*. IntechOpen, 2017. Epub ahead of print. https://doi.org/10.5772/65865
21. Pacheco-Torgal F, Jalali S and Fucic A. *Toxicity of building materials*. 1st ed. Elsevier, 2012.
22. Mandegarian S, Hojjati M and Moghaddar H. Recycled PET foam core sandwich panels with reinforced hybrid composite facesheets: a sustainable approach for enhanced impact resistance. *J Sandw Struct Mater* 2025; 27: 396–428. https://doi.org/10.1177/10996362241298164

23. Khalili P, Skrifvars M, Dhakal HN, et al. Mechanical properties of bio-based sandwich composites containing recycled polymer textiles. *Polymers* 2023; 15(18): 3815. https://doi.org/10.3390/polym15183815, Epub ahead of print 2023.
24. John MJ and John MJ. Design and manufacturing of bio-based sandwich structures. In: *Handbook of composites from renewable materials*. John Wiley & Sons, Ltd, pp. 93–110.
25. Ávila de Oliveira L, Coura GLC, PassaiaTonatto ML, et al. A novel sandwich panel made of prepreg flax skins and bamboo core. *Composites Part C: Open Access* 2020; 3: 100048. https://doi.org/10.1016/j.jcomc.2020.100048
26. Hartoni H, Fajrin J, Anshari B, et al. Effect of core and skin thicknesses of bamboo sandwich composite on bending strength. *Int J Mech Eng Technol* 2017; 8: 12.
27. Santos P, Bouhemame N, Reis PNB, et al. Impact characterization of bio-based sandwich panels with cork core. *Procedia Struct Integr* 2022; 37: 833–840. https://doi.org/10.1016/j.prostr.2022.02.016
28. Ravishankar P, Arya M, Dhakal H, et al. Assessing the mechanical performance of natural fiber thermoplastic composite sandwiches for advanced applications. *Results Mater* 2024; 23: 100600. https://doi.org/10.1016/j.rinma.2024.100600
29. Vinod A, Tengsuthiwat J, Vijay R, et al. Advancing additive manufacturing: 3D-printing of hybrid natural fiber sandwich (Nona/Soy-PLA) composites through filament extrusion and its effect on thermomechanical properties. *Polym Compos* 2024; 45: 7767–7789. https://doi.org/10.1002/pc.28302
30. Buitrago B, Jaramillo F and Gomez M. Some properties of natural fibers (sisal, pineapple, and Banana) in comparison to man-made technical fibers (aramide, glass, carbon). *J Nat Fibers* 2015; 12: 357–367. https://doi.org/10.1080/15440478.2014.929555
31. Nishida H, Carvelli V, Fujii T, et al. Thermoplastic vs. thermoset epoxy carbon textile composites. *IOP Conf Ser Mater Sci Eng* 2018; 406: 012043. https://doi.org/10.1088/1757-899x/406/1/012043
32. Oladele IO, Okoro CJ, Taiwo AS, et al. Modern trends in recycling waste thermoplastics and their prospective applications: a review. *J Compos Sci* 2023; 7(5): 198. https://doi.org/10.3390/jcs7050198, Epub ahead of print 2023.
33. Yang Y, Boom R, Irion B, et al. Recycling of composite materials. *Chem Eng Process Process Intensif* 2012; 51: 53–68. https://doi.org/10.1016/j.cep.2011.09.007
34. Uribe BEB, Soares-Pozzi AC and Tarpani JR. Nanocellulose-coated carbon fibers towards developing hierarchical polymer matrix composites. *Mater Today Proc* 2019; 8: 820–831. https://doi.org/10.1016/j.matpr.2019.02.024
35. Brejcha V, Böhm M, Holeček T, et al. Comparison of bending properties of sandwich structures using conventional and 3D-Printed core with flax fiber reinforcement. *J Compos Sci* 2025; 9(4): 24. https://doi.org/10.3390/jcs9040182, Epub ahead of print 2025.
36. Zhu B, Jiang X, Li S, et al. An overview of recycling phenolic resin. *Polymers* 2024; 16(9): 1255. https://doi.org/10.3390/polym16091255, Epub ahead of print.
37. Birman V and Kardomateas GA. Review of current trends in research and applications of sandwich structures. *Compos B Eng* 2018; 142: 221–240. https://doi.org/10.1016/j.compositesb.2018.01.027
38. Wang Z, Wang C, Gao Y, et al. Porous thermal insulation polyurethane foam materials. *Polymers* 2023; 15(18): 3818. https://doi.org/10.3390/polym15183818, Epub ahead of print.

39. Rede Fde GM. *Desenvolvimento e caracterização de estruturas sanduíche com núcleo honeycomb de cortiça*. Master's Thesis. University of Porto, 2019. https://hdl.handle.net/10216/119408 (accessed 10 April 2025).
40. Amorim Cork Composites. *NL20 Material data sheet*. Santa Maria da Feira, Portugal. https://amorimcorksolutions.com/media/4203/mds-nl20-en.pdf (May 2020, accessed 3 May 2025).
41. King WT, Guin WE, Jordon JB, et al. Effects of honeycomb core damage on the performance of composite sandwich structures. *J Compos Mater* 2020; 54: 2159–2171. https://doi.org/10.1177/0021998319890656
42. Fangueiro R, Velosa JC, van Hattum FWJ, et al. Development of reinforced composite sandwich panels based on 3D fabrics. In: 14th European conference on composite materials - ECCM14, Budapest, Hungary, 7-10 June 2010. https://api.semanticscholar.org/CorpusID:55787699
43. Bos HL, Van Den Oever MJA and Peters OCJJ. Tensile and compressive properties of flax fibres for natural fibre reinforced composites. *J Mater Sci* 2002; 37: 1683–1692. https://doi.org/10.1023/a:1014925621252
44. Amiri A, Ulven CA and Huo S. Effect of chemical treatment of flax fiber and resin manipulation on service life of their composites using time-temperature superposition. *Polymers* 2015; 7: 1965–1978. https://doi.org/10.3390/polym7101493
45. Atalay Kalsen TS, Karadağ HB and Eker YR. The out-of-plane compression behavior of in situ ethylene vinyl acetate (EVA)-Foam-Filled aluminum honeycomb sandwich structures. *Materials* 2023; 16(15): 5350. https://doi.org/10.3390/ma16155350, Epub ahead of print 2023.
46. Ashab ASM, Ruan D, Lu G, et al. Experimental investigation of the mechanical behavior of aluminum honeycombs under quasi-static and dynamic indentation. *Mater Des* 2015; 74: 138–149. https://doi.org/10.1016/j.matdes.2015.03.004
47. Gibson LJ and Ashby MF. *Cellular solids: structure and properties*. 2nd ed. Cambridge University Press, 1997. Epub ahead of print 1997. https://doi.org/10.1017/CBO9781139878326
48. Plantema FJ. *Sandwich Construction: The Bending and Buckling of Sandwich Beams, Plates, and Shells*. New York: John Wiley & Sons, 1966.
49. Lascano D, Guillen-Pineda R, Quiles-Carrillo L, et al. Manufacturing and characterization of highly environmentally friendly sandwich composites from polylactide cores and flax-polylactide faces. *Polymers*2021; 13(3): 342. https://doi.org/10.3390/polym13030342, Epub ahead of print 2021.
50. Stocchi A, Colabella L, Cisilino A, et al. Manufacturing and testing of a sandwich panel honeycomb core reinforced with natural-fiber fabrics. *Mater Des* 2014; 55: 394–403. https://doi.org/10.1016/j.matdes.2013.09.054
51. Sarasini F, Tirillò J, Lampani L, et al. Impact behavior of sandwich structures made of flax/epoxy face sheets and agglomerated cork. *J Nat Fibers* 2020; 17: 168–188. https://doi.org/10.1080/15440478.2018.1477084
52. Jendli Z, Haggui M, Monti A, et al. Experimental analysis of low-velocity impact behaviour on flax-balsa biobased sandwich. *Composites Part C: Open Access* 2024; 14: 100489. https://doi.org/10.1016/j.jcomc.2024.100489

53. Betts D, Sadeghian P and Fam A. Post-impact residual strength and resilience of sandwich panels with natural fiber composite faces. *J Build Eng* 2021; 38: 102184. https://doi.org/10.1016/j.jobe.2021.102184
54. Kelly A and Tyson WR. Tensile properties of fibre-reinforced metals: copper/tungsten and copper/molybdenum. *J Mech Phys Solid* 1965; 13: 329–350. https://doi.org/10.1016/0022-5096(65)90035-9
55. Montreuil A, Mertz G, Bardon J, et al. Flax fiber treatment by an alkali solution and poly(dopamine) coating: effects on the fiber physico-chemistry and flax/elium® composite interfacial properties. *Compos Part A Appl Sci Manuf* 2024; 177: 107963. https://doi.org/10.1016/j.compositesa.2023.107963
56. Allagui S, Mahi AE, Rebiere J-L, et al. Effect of recycling cycles on the mechanical and damping properties of flax fibre reinforced elium composite: experimental and numerical studies. *J Renew Mater* 2021; 9: 695–721. https://doi.org/10.32604/jrm.2021.013586
57. Allagui S, Mahi AE, Rebiere J-L, et al. Experimental studies of mechanical behavior and damage mechanisms of recycled flax/elium thermoplastic composite. *Polym Polym Compos* 2022; 30: 09673911221090048. https://doi.org/10.1177/09673911221090048
58. Bensadoun F, Vanderfeesten B, Verpoest I, et al. Environmental impact assessment of end of life options for flax-MAPP composites. *Ind Crops Prod* 2016; 94: 327–341. https://doi.org/10.1016/j.indcrop.2016.09.006